Global Environmental Change 69 (2021) 102318

Contents lists available at ScienceDirect

Global Environmental Change

journal homepage: www.elsevier.com/locate/gloenvcha

Africa's protected areas are brightening at night: A long-term light pollution monitor based on nighttime light imagery

Zihao Zheng [a,b], Zhifeng Wu [b,c,*], Yingbiao Chen [b], Guanhua Guo [b], Zheng Cao [b], Zhiwei Yang [b], Francesco Marinello [a,*]

[a] Department of Land, Environment, Agriculture and Forestry, University of Padova, Padova, Veneto Region 35020, Italy
[b] School of Geography and Remote Sensing, Guangzhou University, Guangzhou, Guangdong 510006, China
[c] Southern Marine Science and Engineering Guangdong Laboratory (Guangzhou), Guangzhou, Guangdong 511458, China

ARTICLE INFO

Keywords:
Protected areas
Light pollution
Nighttime light
Africa
Human activities

ABSTRACT

As the cornerstone of biodiversity conservation, the core value of protected areas (PAs) is to maintain an area's natural conditions (both day and night) and to restrict human-caused disturbances to biology and the environment. Although the value of PAs has been universally recognized, light pollution within them is worsening as a result of the widespread use of artificial illumination devices. Previous studies have focused on light pollution in PAs and evaluated light radiation using nighttime light imagery. However, given the scale and span of these studies (national scale and over short periods), PA light pollution research should be advanced further. In this paper, we conducted long-term (1992–2018) monitoring and evaluation of light pollution in African PAs using aligned multi-sensor NTL data. The results showed that 1) Africa PAs were impacted by increasingly severe artificial lights during 1992–2018, with all three light indices showing an accelerating increasing trend. 2) The number of light-polluted PAs also rapidly increased, with more than 80% of PAs experiencing aggravated light pollution as of 2018. Different types of PAs had heterogeneous light pollution, which penetrates indiscriminately into all PA regulation levels. 4) Light pollution in African PAs was divided into three types, including outside invasion, internal sources, and mixed pollution. 5) Human activity intensity surrounding the PAs was highly correlated with light pollution within them, with a maximum effect distance of approximately 245 km. This paper provides new approaches for understanding the patterns of light pollution within PAs, and is a valuable reference for future PA planning.

1. Introduction

Since 2015, countries around the world have made progress in promoting global ecological governance but are still far from the climate change reduction and sustainable development goals set out in the Paris Agreement. In particular, global wildlife populations have declined by about 68% due to population expansion, consumption growth, and agricultural reclamation, and there are deep threats and challenges to ecosystem diversity (WWF, 2020). As a positive response to the ecological crisis, the establishment of protected areas (PAs) of various types is a globally recognized conservation strategy that plays a fundamental role in biodiversity and species conservation (Joppa et al., 2008; Watson et al., 2018). PAs are set aside by protocol for special protection and management, such as land or maritime spaces that are representative natural ecosystems, have natural concentrations of rare and endangered species of wild animals and plants, and are natural heritage features of special value (Zhu et al., 2018). Currently, more than 260,000 PAs have been established globally, covering about 15.4% of the Earth's surface area, but this still falls short of the Aichi Biodiversity Targets, which require that at least 17% of the world's land and 10% of the world's oceans be included in PA systems (Cao et al., 2019; Buchanan et al., 2020).

As the cornerstone of biodiversity conservation, the core value of PAs is the maintenance of natural conditions within the area (both day and night) and to prevent and mitigate potential biological and environmental disturbances caused by human activities (Green et al., 2019).

* Corresponding authors at: School of Geography and Remote Sensing, Guangzhou University, No. 230 West Ring Road, Guangzhou Higher Education Mega Center, Guangzhou, China (Z. Wu). Department of Land, Environment, Agriculture and Forestry, University of Padova, Via dell'Università 16, Legnaro, Padova, Italy (F. Marinello).

E-mail addresses: zfwu@gzhu.edu.cn (Z. Wu), francesco.marinello@unipd.it (F. Marinello).

https://doi.org/10.1016/j.gloenvcha.2021.102318
Received 6 December 2020; Received in revised form 21 May 2021; Accepted 28 June 2021
Available online 9 July 2021

Although PA value has been recognized and their numbers are increasing worldwide, these areas still suffer from human interference, including settlement, education, resource development, and tourism activities. It has been reported that globally, more than 6,000,000 km^2 of PAs are exposed to intense human pressures, and more than 50% of PAs have experienced increased human pressures (Jones et al., 2018). Of these disturbances, severe nighttime light pollution has far-reaching biological impacts on species and the ecology, leading to increased attention to the ecological impacts of nighttime light in PAs (Aubrecht et al., 2008; Gaston et al., 2013).

In recent decades, urbanization, population growth, and economic development have led to a rapid and sustained increase in the density and extent of artificial lighting, which has shaped a new global nighttime light environment. The widespread use of artificial light at night has greatly improved human quality of life but also disrupts the natural cycle of light and darkness, which can be regarded as an environmental pressure (Longcore & Rich, 2004; Rich & Longcore, 2006; Navara & Nelson, 2007; Perkin et al., 2011; Mammides, 2020). Ecology and species diversity threats from nighttime light pollution, especially in PAs, are broadly twofold: 1) nighttime lighting affects the abundance, distribution, and ecosystem function of photosensitive species, threatening biodiversity and accelerating species extinction (Aubrecht et al., 2010); 2) nighttime lighting in PAs is typically a sign of greater human activity, which poses a direct threat to the ecological balance and biodiversity (Xiang & Tan, 2017). Therefore, accurate information on the current and historical spatial distribution and intensity of artificial light in PAs is essential for monitoring human activities, assessing the impacts of anthropogenic lighting, and maintaining PA ecology.

Remote sensing, which has the advantages of rapid, macroscopic, and repeatable observations, has become an important technology for PA monitoring and assessments and is widely used worldwide (Green et al., 2019; Riggio et al., 2019; Akodéwou et al., 2020; Dimobe et al., 2017; Zhang et al., 2020). Night light (NTL) remote sensing has been used by scholars to monitor the intensity of human activities and light pollution in PAs because it can directly capture the distribution and intensity of surface artificial light sources on a global scale. Compared to traditional field survey methods, monitoring schemes based on nighttime light remote sensing allow for the quantitative assessment of light pollution and human activities in PAs without "contact" to ecologically sensitive areas (Yang and Xu, 2019). For example, the human stress (footprint) index commonly used by scholars to assess the intensity of anthropogenic disturbance within PAs references lighting data for selected years (Geldmann et al., 2014; Venter et al., 2016; Jones et al., 2018). For time-series monitoring of human activities in PAs, Xiang & Tan (2017) and Shi et al. (2018) used the Defense Meteorological Satellite Program/Operational Linescan System (DMSP/OLS) NTL data to conduct temporal and spatial analyses of light pollution in China's PAs between 1992 and 2012. Xu et al. (2019) used data from a new Visible Infrared Imaging Radiometer Suite Day/Night band (VIIRS/DNB) source to detect NTL disturbance in PAs on mainland China.

In fact, the current widely used and easily accessible NTL products mainly include DMSP/OLS stable light data and NPP/VIIRS cloud-free monthly average composite data, which together comprise NTL observations over a long-time span (1992-present). These previous studies confirmed the potential of NTL data (DMSP/OLS and NPP/VIIRS) for monitoring light pollution in PAs, but to our knowledge, no prior work has joined multi-source NTL data to enable longer time span assessments. Therefore, in this paper, we focused on PAs in the African continent and conducted long-term monitoring and evaluation of light pollution in PAs using aligned multi-sensor NTL data.

2. Materials and methods

2.1. Study area

The African continent covers an area of about 30 million square kilometers (excluding nearby islands), accounting for about 20.2% of the world's total land area, making it the second largest continent in the world after Asia. Meanwhile, Africa is the second most populous continent (1.2 billion) and has an average annual population growth rate of 2.3%. The vast African continent also has a dense concentration of PAs: according to the World Database on Protected Areas (WDPA), there are currently 8,448 PAs in Africa, of which 14.23% and 12.23% are terrestrial and marine, respectively. Considering the size and type of PAs, a total of 2984 PAs, including national, regional, and international designations, were selected in this paper with reference to Xu et al. (2019), as listed in Table 1.

The selected PAs covered all PA types in the IUCN classification system and had a combined area of about 2,880,000 km^2, which is about 10% of the total area of the African continent. PA vector boundaries were derived from the updated database released by the WDPA in August 2020, and based on the original data we made topological corrections to ensure that each patch was as complete as possible and free from overlaps, overhanging points, and other errors. Their locations are shown in Fig. 1.

2.2. Data sources

As opposed to common daytime optical remote sensing, NTL remote sensing has been widely used for monitoring human activities on the ground by effectively capturing faint light emissions at night, including in: urban sprawl and urbanization studies (Lu et al., 2008; He et al, 2006; Yu et al., 2014), population spatial estimates (Sutton, 1997; Zhuo et al., 2009), the spatialization of economic parameters such as GDP (Sutton and Costanza, 2002; Chen and Nordhaus, 2011), electricity consumption and carbon emissions (Elvidge et al., 1997; Ghosh et al., 2010), and fisheries and oil and gas platform detection (Waluda et al., 2004; Cho et al., 1999). Generally, the most frequent and widely used NTL data used by scholars has included DMSP/OLS and NPP/VIIRS products. DMSP/OLS NTL data provide annual synthetic night lighting products from 1992 to 2013, while NPP/VIIRS are monthly synthetic lighting products from 2013 to present (Chen et al., 2019). Despite the differences in sensors and calibrations between the two NTL products, numerous studies have revealed the value and possibilities of using joint multi-source NTL data for surface human activity intensity detection (Li et al., 2017; Wu and Wang, 2019). In this paper, NTL data products from DMSP/OLS and NPP/VIIRS were aligned to enable light pollution detection in African PAs from 1992 to 2018.

Additionally, Sentinel-2 multispectral images were used to investigate the in-situ features of prominent surface light sources, which assisted in classifying the light pollution in Africa's PAs. Detailed parameters of the satellite images are shown in Table 2.

Table 1
Properties of African PAs selected in this paper.

PA Type	IUCN Categories	Count	Area (km^2)
Biosphere Reserve	I_a, II, IV, Not Applicable, Not Reported	44	405,645
Forest Reserve	I_b, II, III, IV, V, VI, Not Applicable, Not Assigned, Not Reported	1766	318,952
National Park	I_b, II, IV, V, VI, Not Assigned, Not Reported	251	725,835
Natural Reserve	I_a, I_b, II, IV, V, VI, Not Assigned, Not Reported	549	190,778
Scenic Site	Not Reported	37	5,237
Wetland Reserve	II, IV, V, VI, Not Reported	203	534,849
Wildlife Reserve	II, III, IV, VI, Not Assigned, Not Reported	92	294,681
World Heritage Site	II, Not Applicable, Not Reported	42	407,758
Total	I_a, I_b, II, III, IV, V, VI, Not Applicable, Not Assigned, Not Reported	2984	2,883,735

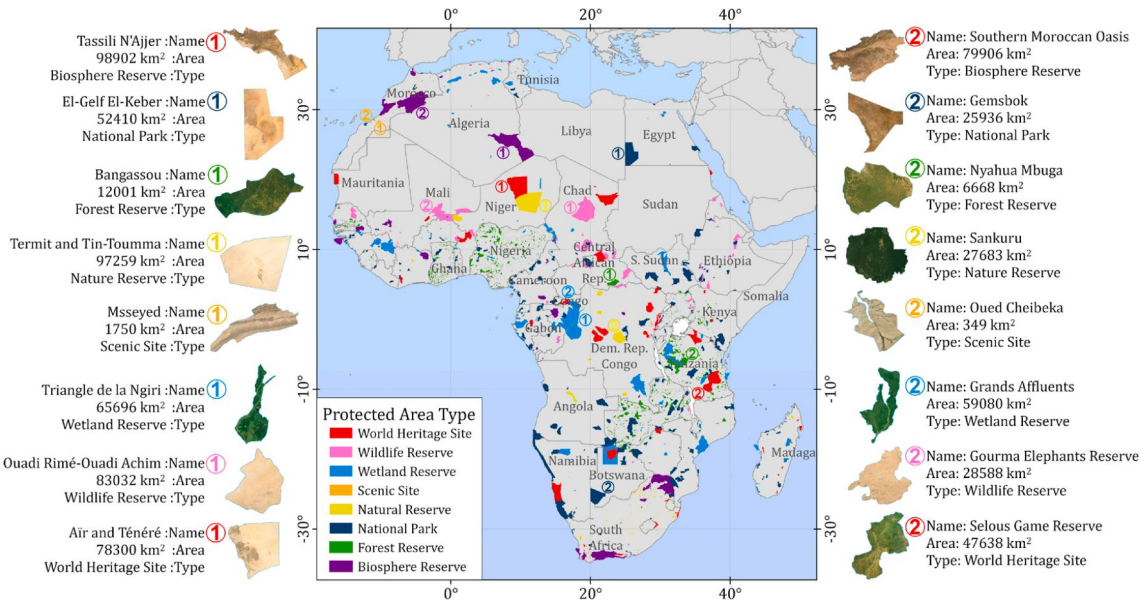

Fig. 1. PA locations in Africa. The left and right panels show thumbnails and information about the top first and second PA within each type, respectively.

Table 2
Spatial and temporal resolution parameters of the satellite images.

Satellite	Sensor	Spatial resolution	Temporal resolution	Data available	Access link
DMSP	OLS	30 arc-second (around 1000 m)	Annual	1992–2013	https://eogdata.mines.edu/products/dmsp/
NPP	VIIRS	15 arc-second (around 500 m)	Monthly	April 2012-Present	https://eogdata.mines.edu/products/vnl/
Sentinel-2	MSI	10 m	5–10 days	June 2015-Present	https://scihub.copernicus.eu/

3. Methods

3.1. Cross-sensor calibration of NTL data

As mentioned earlier, NTL data from DMSP/OLS and NPP/VIIRS differ significantly in terms of temporal coverage and resolution, spatial resolution, radiometric resolution, etc., so pre-processing of the light data is required when they are joined for long-term light pollution studies. In general, the generation of long-term, continuous NTL data includes the following steps: 1) inter-annual calibration of DMPS/OLS data, 2) synthesis of annual VIIRS NTL data, and 3) transformation of VIIRS annual NTL data to align with DMSP/OLS NTL data. Specifically:

Inter-annual calibration of DMPS/OLS NTL data. Annual NTL datasets for 1992–2013, published online by the National Geophysical Data Center (NGDC), are provided by six sensors: F10 (1992–1994), F12 (1994–1999), F14 (1997–2003), F15 (2000–2007), F16 (2004–2009), and F18 (2010–2013). Due to performance differences between sensors and the degradation of the sensors themselves, there is a problem of "light drift" in the time-series NTL dataset (Cao et al., 2015). To eliminate the discontinuity between annual NTL images from 1992 to 2013 and calibrate them, this paper adopted the PBPIF calibration model proposed by Zheng et al. (2019b). This method builds an inter-annual calibration model by automatically detecting the pseudo-invariant feature pixels, which can be efficiently applied to correct large-scale light radiation variability.

Synthesis of annual VIIRS NTL data. The monthly "VIIRS Cloud Mask" NTL product from VIIRS eliminates stray light; however, background noise and outliers still need to be removed. In this paper, we used the method of Zhao et al. (2020) to set thresholds for noise filtering and corrected outliers with the scheme proposed by Shi et al. (2014). Moreover, following the approach of Li et al (2020), annual VIIRS NTL images were synthesized with reference to cloud-free coverage to set weights. Compared with the traditional simple mean composition, the post-weighted synthesis scheme greatly reduced the interference from clouds and solar illumination (Román et al., 2018) and improved data quality.

Align VIIRS annual NTL data to DMSP/OLS data. Aligning heterogenous NTL images has been proposed by several studies (Zheng et al., 2019a; Ma et al., 2020; Hu et al., 2021). Because the annual composite VIIRS NTL data had a better resolution than the OLS annual light data, it was more feasible to align the VIIRS NTL images to the OLS NTL images. Hence, the alignment scheme of Zhao et al. (2020) was used in this paper due to its low input parameters, full-time span, and high robustness. Specifically, the scheme includes three steps: resolution reduction, data structure matching, and automatic pixel alignment. Firstly, the Kernel density (KD) approach was used to transform the resolution from fine to coarse and moderately restore the blurring effect of OLS NTL images. Next, a log-transform was used to aggregate the VIIRS NTL images, as in Eq.1. Finally, a sigmoid function was applied to align the log-transformed images to the OLS NTL images, as in Eq.2.

$$Log^{Y}_{VIIRS_{KD}} = ln\left(VIIRS^{Y}_{KD} + 1\right) \quad (1)$$

$$DMSP^{Y}_{liked} = a + b\left(1/1 + e^{-c\left(Log^{Y}_{VIIRS_{KD}} - d\right)}\right) \quad (2)$$

where $VIIRS_{KD}$ is aggregated VIIRS image of year Y; $Log^{Y}_{VIIRS_{KD}}$ is a log transformed image of $VIIRS_{KD}$; $DMSP^{Y}_{liked}$ is the NTL image for year Y after $Log^{Y}_{VIIRS_{KD}}$ aligned; a, b, c, d are constant values of 6.5, 57.4, 1.9, and 10.8, respectively (Li et al., 2020). In addition, to further optimize the inter-annual light trends, the moving average method was used to eliminate interannual irregular fluctuations in the synthetic light images. Specifically, this paper used a three-year time window to smooth the single-year light images.

3.2. PA lighting change detection

With the advancement of NTL research, especially quantitative NTL

remote sensing studies, several light indices have been widely used to measure surface light pollution and human activities (Ghosh et al., 2009; Wei et al., 2017; Zheng et al., 2020b). In this paper, the total sum of light intensity (TSOL), the mean NTL intensity (MNTLI), and the proportion of lighted area (POLA) were used to measure the light pollution level within PAs. TSOL is defined as the sum of the radiation values for all light pixels in a PA, MNTLI is the mean value of light radiation, and POLA is the proportion of pixels with a digital number (DN) greater than 1.

Furthermore, Theil-Sen Median trend analysis and the Mann-Kendall test were used to examine trends in the long-term sequence of light intensity changes in PAs. Both methods have a strong tolerance for outliers and are important for conducting trend analysis of time series data. They have been widely used to analyze trends in vegetation, precipitation, air temperature, and other intermediate factors (Tucker et al., 1991; Liu et al., 2011). The Theil-Sen Median trend analysis formula is:

$$Slope_{NTL} = median\left(\frac{NTL_j - NTL_i}{j - i}\right) 1992 \le i \le j \le 2018 \quad (3)$$

where NTL_i and NTL_j are pixel NTL values at year i and j, respectively. When $Slope_{NTL} > 0$, the light intensity is increasing at the pixel; otherwise, it is decreasing.

The Mann-Kendall test is calculated as:

$$Z = \begin{cases} (S-1)/\sqrt{Var(S)} & (S > 0) \\ 0 & (S = 0) \\ (S+1)/\sqrt{Var(S)} & (S < 0) \end{cases} \quad (4)$$

$$S = \sum_{i=1}^{n-1} \sum_{j=i+1}^{n} sgn(NTL_j - NTL_i) \quad (5)$$

$$sgn(NTL_j - NTL_i) = \begin{cases} 1 & (NTL_j - NTL_i > 0) \\ 0 & (NTL_j - NTL_i = 0) \\ -1 & (NTL_j - NTL_i < 0) \end{cases} \quad (6)$$

$$Var(S) = n(n-1)(2n+5)/18 \quad (7)$$

where *sgn* is symbolic function; *n* is the length of the time series; *Z* is the significance test statistic with a value range of $(-\infty, +\infty)$. At a confidence level of $\alpha = 0.05$, $|Z| \ge Z_{\frac{0.05}{2}} = 1.94$ indicates that there is a significant change in the light intensity.

4. Results

4.1. Light pollution dynamics of PAs

Time-series remote sensing monitoring is an effective way to track the dynamics of light pollution and anthropogenic disturbance within PAs. Hence, we used nighttime light remote sensing observations to assess the dynamics of light pollution in African PAs over the past 26 years at the general, PA, and pixel levels.

4.1.1. Index dynamics at the general level

The results for tracking light pollution in African PAs based on NTL images from 1992 to 2018 are shown in Fig. 2. It is worth noting that, despite the pre-processing procedures that were adopted in this paper to align the two light data sources, in faintly lighted PAs (as opposed to urban areas), the significant improvement in VIRS sensor radiance resolution allowed it to record more light radiation and resulted in a "jumping" phenomenon in 2013 (see further discussion in section 5.1). Specifically, the three lighting indices (MNTLI, TSOL, and POLA) in Fig. 2 all increased with time, although there was a clear break between 1992 and 2012 and 2013–2018. We eliminated this statistically unexpected shift by 1) assuming that PA light radiation in 2013 would continue the trend from 1992 to 2012, and 2) converting between observed and predicted light radiation values in 2013 to correct the light radiation in subsequent years. The green scatter plot in Fig. 2 shows the adjusted PA light index values, which steadily increased from 1992 to 2018 in the African PAs. Generally, over the past 26 years, African PAs experienced a dramatic increase in nighttime light pollution, with TSOL spiking from 446,010 to 2291253, MNTLI jumping from 0.15 to 0.78, and POLA increasing from 1.39% to 6.19% within PAs.

4.1.2. MNTL dynamics at the PA level

At the reserve level, the MNTLI of each PA was calculated annually because it better reflects the level of light pollution (Xu et al., 2019). The results in Table 3 show that only 0.87% of the PAs mitigated light pollution over the past 26 years, 18.06% had no change in light radiation, and 81.07% were under pressure to increased light pollution. Notably, of the 2,419 PAs that experienced increased light pollution, approximately 82% did not suffer from light pollution in 1992 but did have light pollution in 2018, which we referred to as primary pollution. About 18% of the PAs observed light radiation in 1992 and detected even higher light radiation in 2018, which we referred to as secondary pollution.

In addition, to further reveal the spatial characteristics of light pollution dynamics in PAs, we analyzed spatial autocorrelation at the PA level. The results of Global Moran's I (0.21, $p < 0.01$) indicated that there was a significant spatial clustering effect of light pollution dynamics over the past 26 years. More specifically, we found that PAs with high pollution increases were mainly concentrated along the Mediterranean coast, south of the Sahel and in the Great Lakes region, whereas

Table 3
Statistics of light radiation changes in African PAs.

Dynamics	Number of PAs			Percent (%)	
	Count				
Light decrease	26			0.87	
No-light increase	539			18.06	
Light increase	Primary pollution	1978	2419	66.29	81.07
	Secondary pollution	441		14.78	

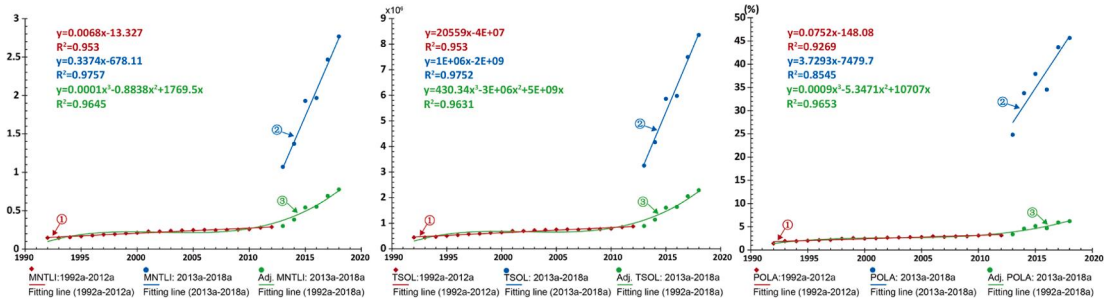

Fig. 2. Dynamic changes in TSOL, MNTLI, and POLA values in the studied PAs. Red symbols represent OLS observations, blue symbols represent VIIRS observations, and green symbols represent the corrected results. (For interpretation of the references to colour in this figure legend, the reader is referred to the web version of this article.)

low pollution increases were concentrated in the Sahara Desert, the Congo Basin, etc., where the environment was extremely harsh or pristine (Fig. 3). We hypothesize that landscape habitability was one of the driving forces that shaped this distribution, as a more livable environment will lead to higher population density and human activity, and generate more artificial lighting that threatens the darkness of the reserve.

4.1.3. Light intensity dynamics at the pixel level

At the pixel level, we performed Theil-Sen Median trend analysis and Mann-Kendall tests to detect dynamic changes in light radiation for PA light pixels between 1992 and 2012 and 2013–2018 (Fig. 4). From 1992 to 2012, 55,421 and 14,539 pixels had significant increases and decreases in light radiation, respectively, with a mean value of 0.23 for Sen's slope. From 2013 to 2018, respective increases and decreases were 971,788 and 60,195 with a significant mean value of 0.78 for Sen's slope. Although differences in sensor performance resulted in many more observed pixels with light radiation change from 2013 to 2018 than from 1992 to 2012, the sharp increase in pixels with more light radiation and Sen's slope values over the two periods confirmed that African PAs have experienced increasing light pollution over the last 26 years.

4.2. Categorized light pollution of PAs

4.2.1. Categories for different design purposes

The PAs selected in this paper were divided into eight categories (Tab.1) according to their design purpose, and analysis of the pollution differences between the types will help us to better understand the structural characteristics of light pollution. Fig. 5 shows the MNTLI values for different PA types in 1992, 2012, 2013, and 2018. The results showed that 1) in 2018, forest reserves, biosphere reserves, wetland reserves, and scenic sites had substantially higher MNTLI values than the other reserve types, and there were significant differences in light radiation between them. 2) All types experienced an increase in light radiation during both OLS and VIIRS observations, and the most significant increases were observed at scenic sites and wetland reserves, with respective increases of 122% and 148% from 1992 to 2012, and 284% and 181% from 2013 to 2018. Meanwhile, the natural reserves and World Heritage Sites had the smallest increases of 82% and 23% from 1992 to 2012, and 98% and 117% from 2013 to 2018, respectively.

In addition, pixel-scale trend analyses and tests showed that the light radiation Sen's slope values for scenic sites, biosphere reserves, and wetland reserves exceeded 0.2 in the OLS observation period and 0.8 in the VIIRS observation period, further confirming that those types experienced dramatic light radiation growth over the past 26 years. In general, there were differences in light pollution between the different types of reserves, with scenic sites, biosphere reserves, and wetland reserves experiencing particularly severe light pollution and also faster increases in light radiation.

4.2.2. Categories for different levels of regulation

The PA catalogue system developed by the International Union for Conservation of Nature (IUCN) classifies PAs according to their management objectives and has been endorsed by international agencies such as the United Nations and many national governments as the global standard for defining and documenting PAs. Currently, there are six types of IUCN catalogue systems, including: I_a (Strict Nature Reserve), I_b(Wilderness Area), II (National Park), III (Natural Monument or Feature), IV (Habitat/Species Management Area), V (Protected Landscape/Seascape) and VI (PA with sustainable use of natural resources). Previous studies have already identified a relationship between human activity intensity and PA control level, with strictly controlled PAs (IUCN categories I and II) generally experiencing lower human activity pressures (Jones et al., 2018).

Fig. 6 shows MNTLI values for PAs in different years under the IUCN catalogue system. Firstly, during the period from 1992 to 2012, the overall level of light radiation in PAs was low and light radiation in IUCN-listed PAs was significantly lower than in PAs that were not included in the category (not applicable, not assigned, and not reported). Secondly, from 2013 to 2018, light radiation in PAs at all regulatory levels increased substantially, but the difference in light radiation between IUCN-listed and not-included PAs decreased.

Contrary to the well-known belief that human pressure on PAs decreases as control level increases, our monitoring of light pollution and Sen's slope (Table 4) under the IUCN catalogue showed that the current light pollution intensity was less correlated with control level and instead penetrated all PAs indiscriminately. For instance, I_a, as the most strictly regulated PA category, should theoretically be exposed to the lowest levels of human stress and light pollution, yet significant increases in MNTLI were observed during the study period and the light pollution problem was quite serious.

4.3. Links between human activity and light pollution in PAs

On the one hand, night light basically comes from artificial light sources associated with human activities, and on the other, most human activities tend to aggregate and expand. Therefore, exploring the relationship between human activities outside PAs and light pollution in them can help us better optimize PA planning strategies to minimize environmental disturbance.

To generate layers that characterized human activity level, this paper first synthesized an intensity map of human activity on the African continent in 2018 based on land use data and lighting data. Specifically:

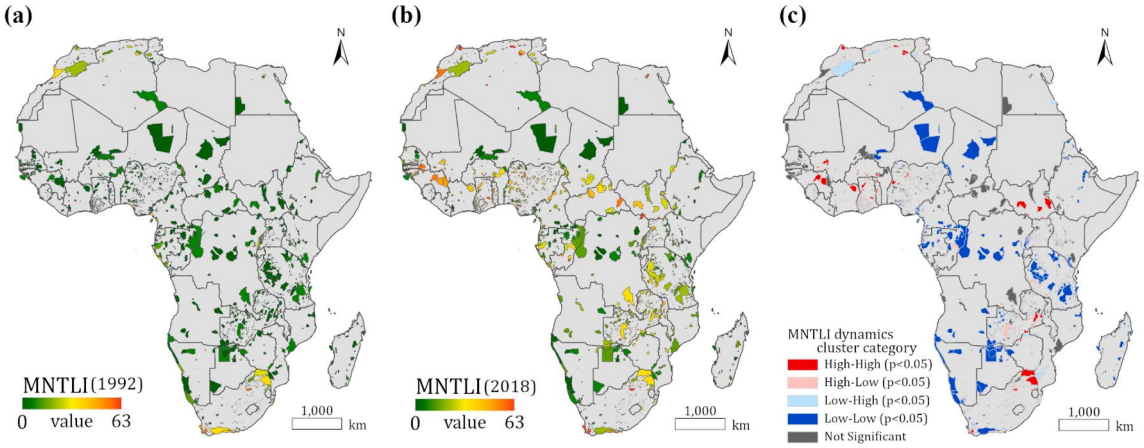

Fig. 3. Spatial distribution and clustering characteristics of MNTLI in PAs.

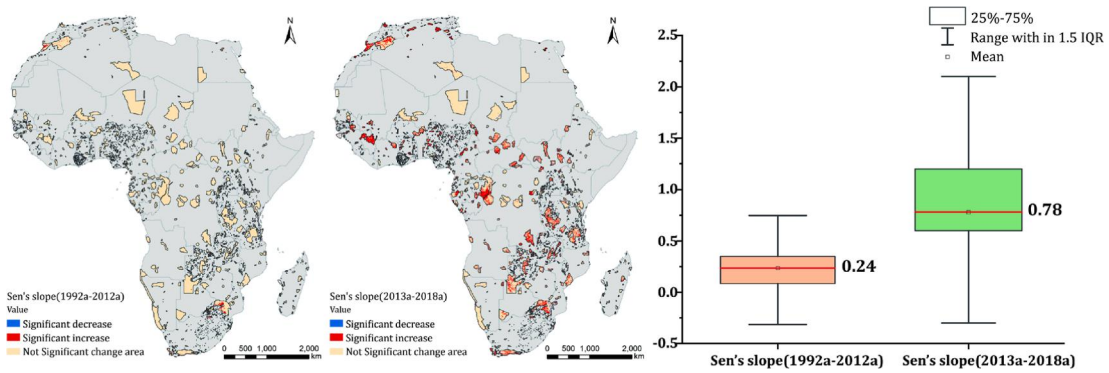

Fig. 4. Sen's slope results during the OLS and VIIRS observation periods.

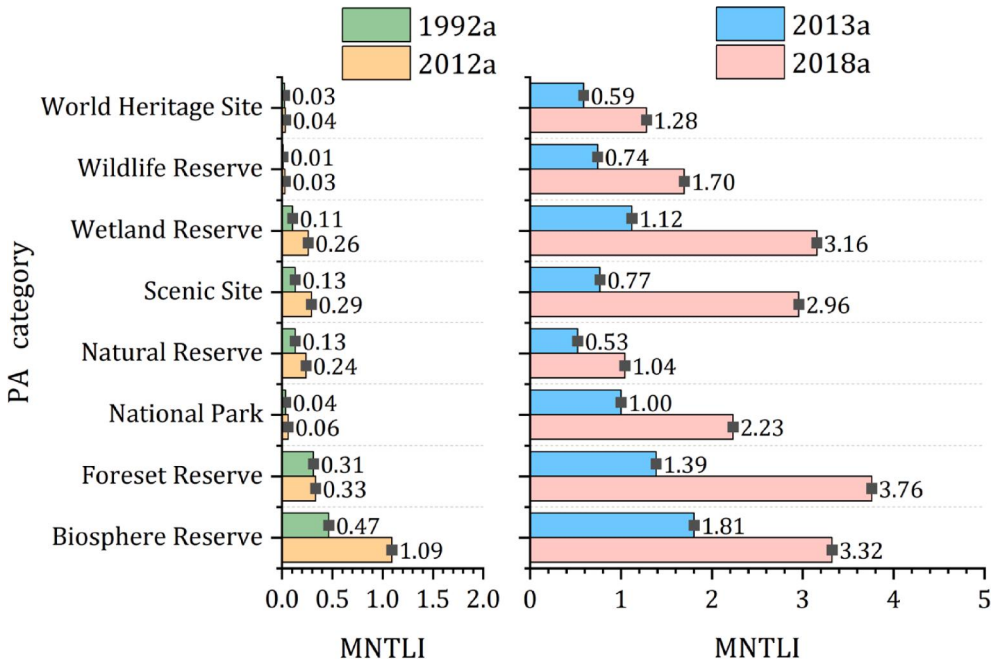

Fig. 5. MNTLI values for different PA types in 1992, 2012, 2013, and 2018.

1) built-up land intensity was extracted based on the land cover classification product CGLS-LC100 collection 3 (Buchhorn et al., 2020) under Copernicus Global Land Service; 2) the mean values of the built-up land intensity layer and the 2018 NTL images were calculated and exported as the African continent human activity intensity map. The derived intensity map contained observations of human activities on the ground from daytime optical remote sensing and NTL remote sensing, which were able to accurately measure the human activity levels in the area. Based on the above layers, we carried out quantitative assessments of the human activity impact on PA light pollution.

PA perspective. According to the average size of the protected area and the human activity footprint, we constructed buffer zones around PAs at thresholds of 100 km, 200 km, and 300 km, and calculated the human activity intensity within them (Fig. 7-a). Then, average human activity intensity within different buffer distances under the light pollution gradient was calculated and the results are shown in Fig. 8. The results showed that 1) more severe light pollution was associated with higher human activity intensity around the PAs, and this pattern was stable across multiple buffer distances; 2) for a PA with the same level of light pollution, the detected surrounding human activity intensity increased as the buffer zone expanded (100–300 km). One well-known phenomenon is that light has a serious halo effect, especially for high-intensity radiation sources at night (Abrahams et al., 2018, Zheng et al., 2020a). Therefore, compared to light sources inside the reserve, the afterglow from artificial light sources outside the reserve was another key source of PA light pollution that cannot be ignored.

Human activity perspective. The PAs perspective was essentially a "results-conditions" perspective; that is, the differences in results were compared to differences in conditions, which revealed that external human activities were a key driver of light pollution in PAs. Hence, to compare the contribution of different conditions (human activity level outside the PAs) to results (light pollution inside the PAs), we designed a stepwise approximation strategy based on buffer distance. This identified the critical distance for the effect of external human activities on light pollution inside the PA (Fig. 7-b). Theoretically, within the scope of human activity, human activity intensity and light pollution of PAs should have a significant positive correlation, i.e., higher intensity human activities around the PA would cause more serious light pollution within it. Therefore, we created multiple buffers and computed light radiation values of PAs under the human activity intensity gradient until the positive correlation between them was unstable (Fig. 9). The comparisons at different buffer distances showed that closer sources of high-intensity human activity led to stronger light emission in the PA. We also used stepwise approximation to determine that a positive correlation

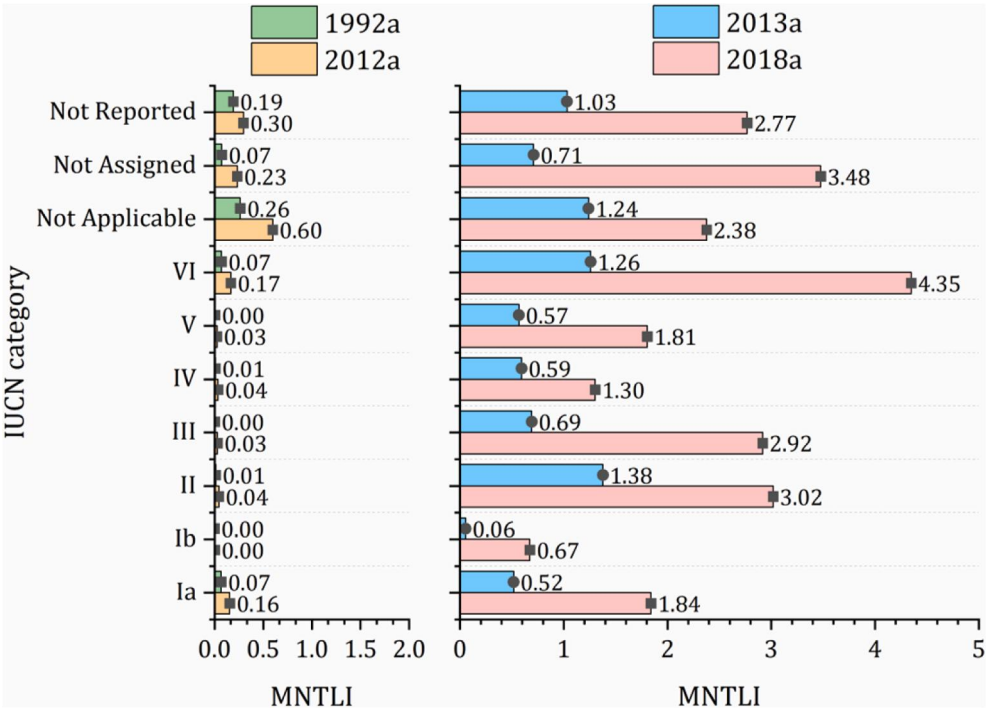

Fig. 6. MNTLI values for different PA regulation levels in 1992, 2012, 2013, 2018.

Table 4
Sen's slope under different PA types and IUCN categories.

PA Category	Sen's slope 1992–2012	2013–2018	IUCN Category	Sen's slope 1992–2012	2013–2018
Forest Reserve	−0.16	0.83	I_a	0.67	0.91
Wildlife Reserve	0.10	0.77	I_b	0.07	0.67
National Park	0.17	0.72	II	0.17	0.76
Natural Reserve	0.19	0.75	III	0.13	0.91
World Heritage Site	0.25	0.74	IV	0.20	0.74
Scenic Site	0.21	0.95	V	0.03	0.80
Biosphere Reserve	0.29	0.82	VI	0.23	0.96
Wetland Reserve	0.27	0.80	Not Applicable	0.29	0.80
			Not Assigned	0.26	0.73
			Not Reported	0.12	0.79

between external human activities and light pollution within the PA was not valid beyond a buffer distance of 245 km. Therefore, it can be assumed that a 245 km radius around the PA is a potential threshold for the disturbance effects that high-intensity human activity sources would cause in a PA.

5. Discussion

5.1. Light pollution characteristics of PAs

As the immense value of PAs in maintaining natural habitats and conserving biodiversity has been recognized worldwide, the number of PAs has increased to 260,000. Nevertheless, there are still a considerable number of PAs that face intrusion from artificial light sources at night. All three light indices in our study confirmed that light pollution pressures on the African continent's PAs have been rising since 1992 at an increasing rate. It should be emphasized that this increase in light pollution in PAs has been comprehensive. On the one hand, light radiation values increased, with MNTLI surging from 0.15 to 0.78 between 1992 and 2018. On the other hand, the number of light-polluted PAs also climbed, with more than 80% of PAs suffering from varying degrees of light pollution in 2018. Meanwhile, according to World Bank statistics, sub-Saharan Africa's population and total GDP respectively increased approximately two and four times between 1992 and 2018. The population boom and dramatic economic growth have accelerated the intensity and scope of human activities in Africa, and threats to PAs are increasingly evident.

As a positive response to potential human activity disturbance in PAs, the IUCN catalogue system classified PAs into different regulation levels. The implementation of the IUCN classification system did appear to have a positive effect on restricting human activities and light pollution in PAs. Fig. 6 clearly shows that from 1992 to 2012, light pollution in PAs under the IUCN control system was significantly lower than in non-regulated areas (one-way ANOVA $p < 0.01$). However, this regulation appeared to be ineffective in more recent years (p greater than 0.1), and increased slightly in PAs under the IUCN classification system, with some types even exceeding non-regulated PAs.

Although the high-performance photo-multiplier tube (PMT) used for nighttime remote sensing can detect faint light on the earth's surface, due to the single-band and coarse spatial resolution the NTL imagery still cannot accurately identify the in-situ light source characteristics. Also, since PMT was only sensitive to actively radiating light sources, a large number of non-actively radiating background features could not be recorded, whereas background information was crucial for identifying

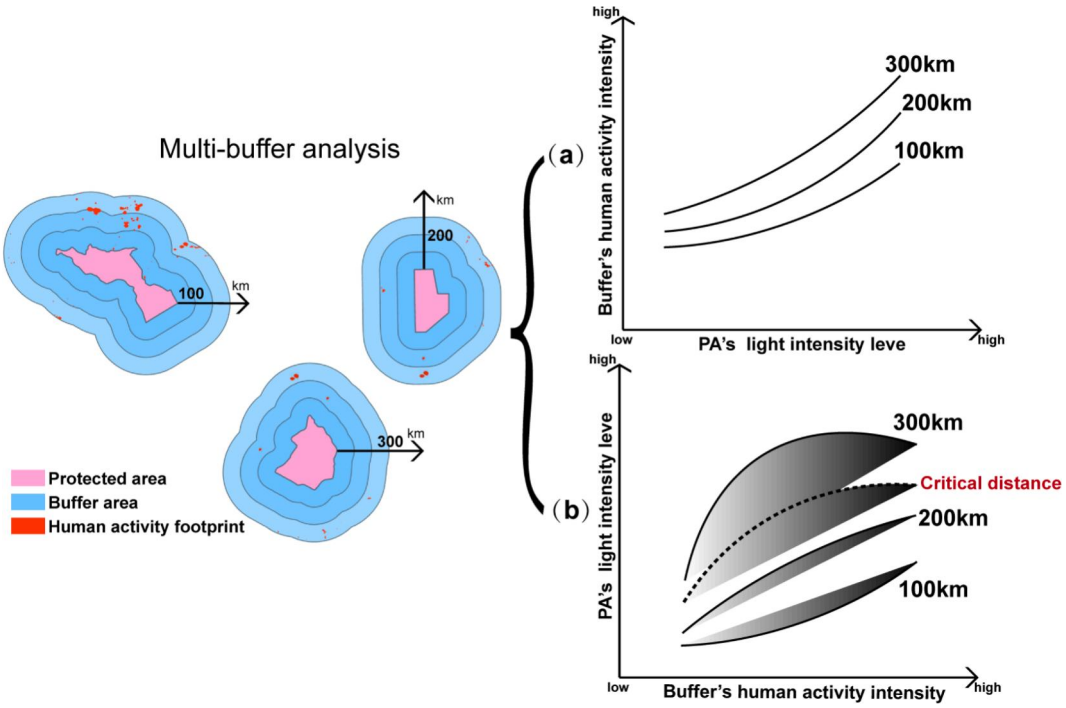

Fig. 7. Diagram of the multiple buffer analysis conducted at PA peripheries.

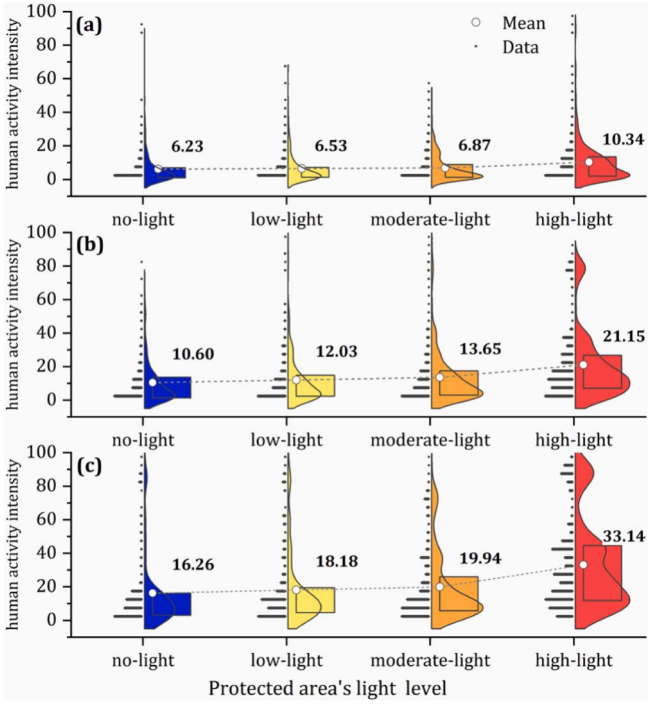

Fig. 8. Human activity intensity under light pollution gradients in PAs at different buffer distances.

the characteristics and types of surface light emission sources. Considering these deficiencies of nighttime light remote sensing, joint daytime high-resolution optical observation for feature identification is a feasible solution. By comparing the spatial distribution between the surrounding background features (especially artificially modified surfaces) and the sources of light radiation at night in a PA, we can identify the light pollution sources. We used high-resolution Sentinel-2 imagery to conduct a visual inspection of PAs that were exposed to moderate and high-intensity light pollution (~50%). According to the spatial locations of light emission sources within the PA, we found that the current light pollution intrusion could be roughly divided into three categories: 1) **Outside invasion type** (Fig. 10-a). For this type, PAs were usually located around (or even within) cities, where the human activity intensity within the PA was low; however, due to the halo and radiation effects of city lights, high levels of light pollution were observed within the PA. 2) **Internal Sources type** (Fig. 10-b). This type of PA was usually not surrounded by high light pollution sources represented by cities, but human activities within them (e.g., construction, agricultural facilities, etc.) contributed to light pollution. 3) **Mixed Pollution Type** (Fig. 10-c). This type included both forms of pollution described above, where the PA was subjected to high-intensity light pressure from the surrounding area and was also affected by internal human activities.

In fact, we contend that the key factor that shaped the three different types of PA light intrusion described above was the distance from the PA to high-intensity anthropogenic areas (e.g., cities). PAs closer to cities were more susceptible to urban light radiation, even with the intrusion of urban land, which worsened the light pollution problem. For PAs far from cities, light pollution was mostly associated with partially built-up land and agricultural facility development. The subsequent multiple-buffer analysis also supported our view that human activity intensity surrounding PAs was positively correlated with light pollution, and this correlation stabilized at a radius of 245 km. This meant that human activities within 245 km of PAs had a strong impact on light pollution within PAs, but the impact did not increase beyond this threshold. The clarification of the distance threshold will allow us to better avoid the interference of human activities on the night ecology of PAs.

5.2. Potential and challenges of aligned NTL data for light pollution studies in PAs

Currently, the two main sources of light data are OLS and VIIRS sensors. These differ in both spatial and radiometric resolution, which has become one of the limitations in long-term PA light pollution studies. Therefore, to achieve long-term sequential light pollution monitoring, this paper adopted the time-continuous NTL dataset developed by Li et al. (2020) and further optimized it using a moving

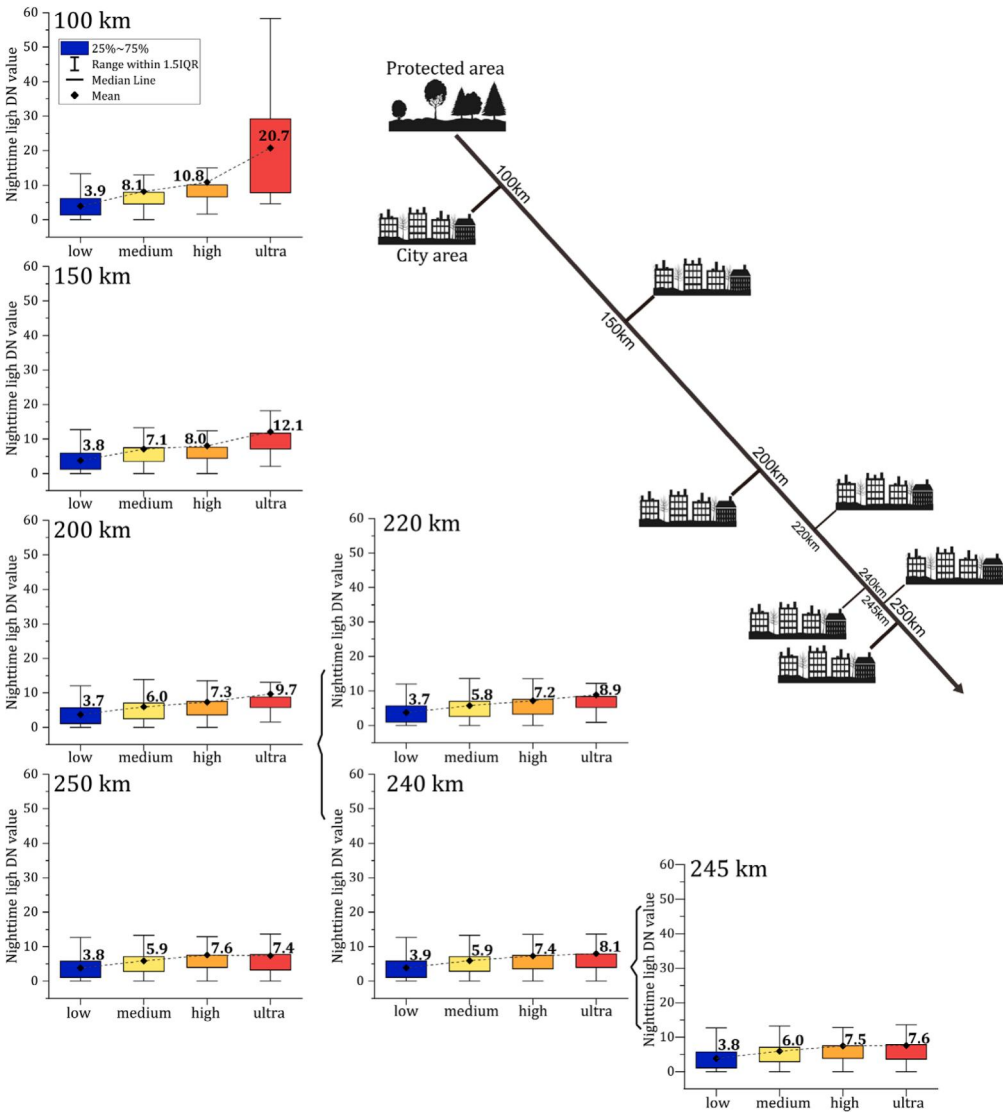

Fig. 9. Correlations between human activities and light pollution in PAs within different distances. When the buffer distance is<250 km, the higher the intensity of human activities, the larger the light DN values. When the buffer distance is 250 km, the light DN value under the ultra-high level of human activity intensity is less than that under high level of human activity intensity.

window. Although the dataset had good spatial continuity and stability (Li et al., 2020; Zhao et al., 2020), there are still several limitations that need to be addressed.

First, the radiation "drift" in low-light regions. Although increasing light pollution was detected in the PA, there was still a large light radiation gap compared to the urban areas. With the "faint" light background in PAs, the difference in sensor performance was further amplified, and numerous faint light pixels that were not recorded by OLS sensors were captured by VIIRS. In addition, the S-function used to convert VIIRS to DMSP-liked data compressed pixel values in the low-light radiation interval, resulting in overestimation in the converted light image (Zhao et al., 2020). To confirm our speculations and measure light radiation dynamics, we selected four sample areas in the African region with different levels of development (Fig. 11). In areas with strong background light radiation, such as Cairo and Lagos, the light radiation clearly increased throughout the study period, especially during 2012–2013 (the junction of the two light datasets) with a smooth shift. In areas without background light radiation, such as maritime space, the light radiation remained at zero over the study period. In PAs with low light radiation, the light radiation curve after moving window smoothing still jumped, especially in 2012–2013. For PA light pollution monitoring, although this spike in radiation resulted in higher light pollution levels in 2013–2018 than in 1992–2012, we considered this partial overestimation to be acceptable, especially since we used a segmented comparison strategy to circumvent possible overestimation.

Second, VIIRS data exhibit seasonal effects. As mentioned earlier, because the VIIRS lighting data products are distributed monthly, light radiation differences are observable every month. Previous studies have shown that there is a clear relationship between monthly light radiation changes and surface vegetation, as well as snow cover changes, especially in urban areas, which need to be considered when conducting a light radiation trend analysis using the VIIRS product (Levin, 2017; Zheng et al., 2019a). Considering the climatic conditions and geographical location of African PAs (more than 90% located at low latitudes, no snow cover, low monthly variation of vegetation, and far from urban areas), we believed that the weak seasonal effect of VIIRS light radiation in PAs could be ignored. In addition, the post-weighted annual synthetic method we adopted could further reduce the seasonal effect and improve the stability of the model.

Third, there was a pixel blooming effect (PiBE). PiBE is a unique effect of nighttime light images, which negatively impacts NTL-based analyses (Henderson et al., 2003). In response, several scholars have

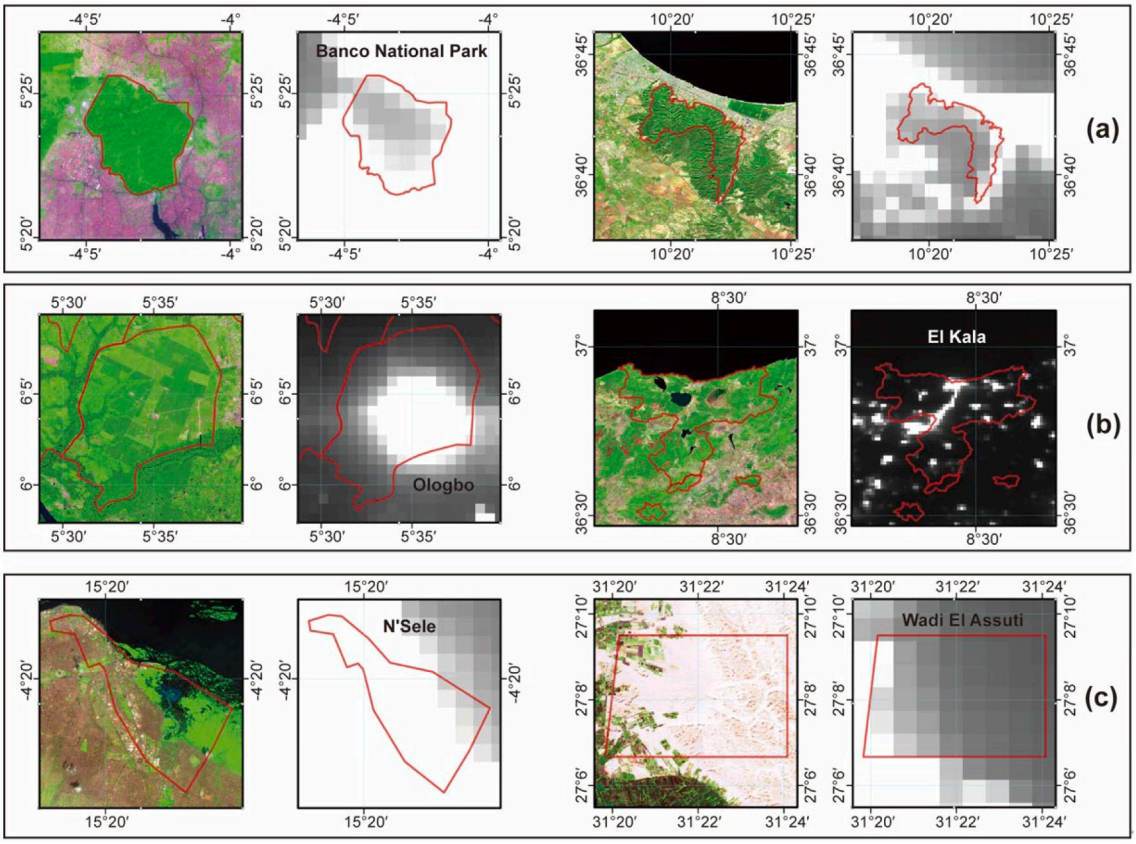

Fig. 10. Three types of light intrusio in PAs.

proposed de-ambiguous, PiBE-free models to mitigate or even eliminate PiBE with good results (Abrahams et al., 2018). However, it should be noted that in this paper we did not adopt the corresponding methods to suppress PiBE manually due to the following considerations. The first was the specificity of the study area. The most prominent problem posed by PiBE in NTL-based analysis is the introduction of pseudo-light pixels in non-built-up areas, which typically causes the urban area being extracted to be overestimated. However, for African PAs, the impervious surface fraction (ISF) remained at quite low levels despite ongoing human intrusion, suggesting the absolute PiBE intensity of PAs was less than in high- ISF regions (Zheng et al., 2020a). Second, this study's core aim was to capture light pollution in PAs, which differed from the classical light-based urban area and urbanization index mapping. In fact, PA light pollution did not only come from internal radiation sources but also from a large number of external artificial light facilities, whose halos still illuminated the night sky of the PA and disturbed the environment. Therefore, it is crucial to retain these PIBE generated halos to inform our results without underestimating the true light pollution levels in PAs. Third, this paper was a time-series study based on aligned NTL data and PiBE was observed every year, which meant that the disturbance caused by PiBE could be offset to a considerable extent during the trend analysis.

5.3. Further research

In this paper, we conducted a long-term monitoring study of light pollution in PAs on the African continent by combining light data from two sensors, DMSP/OLS and NPP/VIIRS. Although the results of the study contribute to the understanding of light pollution, types, and differences in PAs, there are still some aspects that deserve to be further understood and improved. First, to enable light pollution monitoring across long time spans, an aligned VIIRS to OLS conversion scheme was utilized. Although this scheme had good continuity in urban and non-lighted areas, there was still a "radiation jump" in PAs. Therefore, data continuity correction in a low light radiation background should be conducted to obtain more accurate and consistent light pollution monitoring. Second, we selected only PAs that were land-based and larger than 10 km^2 in Africa, which meant that our results ignored smaller, island- and marine-based PAs. Third, our study of disturbance distances to PAs considering surrounding human activities was a data-driven exploration that lacked mechanistic analysis. This prompts us to utilize more powerful spatial analytical models (like gravitational models) for mechanistic studies of representative PAs in future studies.

6. Conclusion

In this paper, we extracted a nighttime light image sequence for the period from 1992 to 2018 within African PAs using aligned DMPS/OLS and NPP/VIIRS NTL products, and carried out the first light pollution assessment of PAs. Despite the spatial and radiometric domain uncertainties in current light data products, our qualitative and quantitative investigation confirmed the dynamics of light pollution in African PAs. The results of our study showed that African PAs have experienced increasing artificial light invasion from 1992 to 2018. On the one hand, the total amount of light radiation (three light indices) has steadily increased, and on the other hand, the extent of light pollution also expanded significantly, with more than 80% of PAs currently suffering from increased pressure from artificial lights. In addition, it was found that light pollution heterogeneity existed across different types of PAs, with scenic sites, biosphere reserves, and wetland reserves having particular exposure. Relatively speaking, the correlation between light pollution intensity and regulation levels in PAs was weakening, and light pollution penetrated indiscriminately into all levels. Finally, our assessment of the intensity of human activities around PAs and light

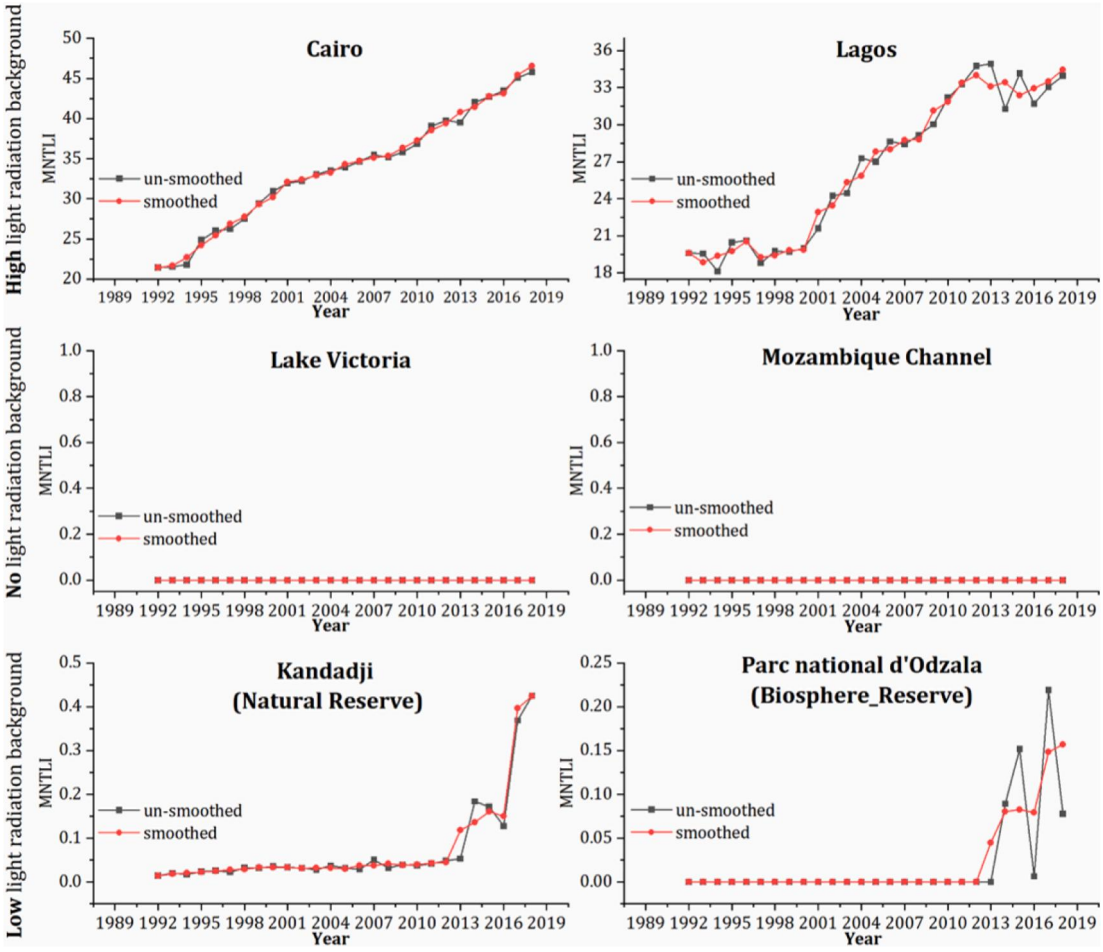

Fig. 11. NTL radiance dynamics across multiple backgrounds.

radiation within them identified a strong positive correlation between human activities and light pollution that stabilized with distance, with a maximum effect at approximately 245 km. More generally, this study offers insights into the status and dynamics of light pollution in African PAs. Furthermore, distance thresholds for anthropogenic effects can be utilized in future PA planning and urban expansion.

CRediT authorship contribution statement

Zihao Zheng: Conceptualization, Methodology, Software, Validation, Investigation, Writing - original draft. **Zhifeng Wu:** Supervision, Project administration, Funding acquisition. **Yingbiao Chen:** Writing - review & editing. **Guanhua Guo:** Writing - review & editing. **Zheng Cao:** Writing - review & editing. **Zhiwei Yang:** Software, Validation. **Francesco Marinello:** Conceptualization, Supervision, Project administration, Writing - review & editing.

Declaration of Competing Interest

The authors declare that they have no known competing financial interests or personal relationships that could have appeared to influence the work reported in this paper.

Acknowledgments

The authors appreciate constructive comments by the associate editor and anonymous reviewers. This research was financially supported by the National key R&D Program of China (No. 2018YFB2100702), Key Special Project for Introduced Talents Team of Southern Marine Science and Engineering Guangdong Laboratory (Guangzhou) (No. GML2019ZD0301) and NSFC-Guangdong Joint Fund (No. U1901219).

References

Abrahams, A., Oram, C., Lozano-Gracia, N., 2018. Deblurring DMSP nighttime lights: A new method using Gaussian filters and frequencies of illumination. Remote Sens. Environ. 210, 242–258. https://doi.org/10.1016/j.rse.2018.03.018.

Akodéwou, A., Oszwald, J., Saïdi, S., Gazull, L., Akpavi, S., Akpagana, K., Gond, V., 2020. Land use and land cover dynamics analysis of the Togodo protected area and its surroundings in Southeastern Togo. West Africa. Sustainability 12 (13), 5439. https://doi.org/10.3390/su12135439.

Aubrecht, C., Elvidge, C., Ziskin, D., Longcore, T. and Rich, C., 2008. 'When the Lights Stay On' - A Novel Approach to Assessing Human Impact on the Environment. Retrieved May 10, 2021, from. https://earthzine.org/when-the-lights-stay-on-a-novel-approach-to-assessing-human-impact-on-the-environment/.

Aubrecht, C., Jaiteh, M., Sherbinin, A., 2010. Global Assessment of Light Pollution Impact on Protected Areas. Retrieved May 10, 2021, from. http://www.ciesin.columbia.edu/documents/light-pollution-Jan2010.pdf.

Buchanan, G.M., Butchart, S.H.M., Chandler, G., Gregory, R.D., 2020. Assessment of national-level progress towards elements of the Aichi Biodiversity Targets. Ecol. Ind. 116, 106497. https://doi.org/10.1016/j.ecolind.2020.106497.

Buchhorn, M., Smets, B., Bertels, L., De Roo, B., Lesiv, M., Tsendbazar, N., Linlin, L., Tarko, A., 2020. Copernicus Global Land Service: Land Cover 100m: Version 3 Globe 2015–2019: Product User Manual. Zenodo. https://doi.org/10.5281/zenodo.3606295.

Cao, W., Huang, L., Xiao, T., Wu, D., 2019. Effects of human activities on the ecosystems of China's National Nature Reserves. Acta Ecologica Sinica 39 (04), 1338–1350. https://doi.org/10.5846/stxb201808251814.

Cao, Z., Wu, Z., Kuang, Y., Huang, N., 2015. Correction of DMSP/OLS night-time light images and its application in China. Journal of Geo-information Science 17 (9), 1092–1102. https://doi.org/10.3724/SP.J.1047.2015.01092.

Chen, X., Nordhaus, W.D., 2011. Using luminosity data as a proxy for economic statistics. Proceedings of the National Academy of Sciences 108 (21), 8589–8594. https://doi.org/10.1073/pnas.1017031108.

Chen, Y., Zheng, Z., Wu, Z., Qian, Q., 2019. Review and prospect of application of nighttime light remote sensing data. Progress in Geography 38 (02), 205–223. https://doi.org/10.18306/dlkxjz.2019.02.005.
Cho, K., Ito, R., Shimoda, H., Sakata, T., 1999. Technical note and cover fishing fleet lights and sea surface temperature distribution observed by DMSP/OLS sensor. Int. J. Remote Sens. 20 (1), 3–9. https://doi.org/10.1080/014311699213569.
Dimobe, K., Goetze, D., Ouédraogo, A., Forkuor, G., Wala, K., Porembski, S., Thiombiano, A., 2017. Spatio-Temporal Dynamics in Land Use and Habitat Fragmentation within a Protected Area Dedicated to Tourism in a Sudanian Savanna of West Africa. Journal of Landscape Ecology 10 (1), 75–95. https://doi.org/10.1515/jlecol-2017-0011.
Elvidge, C.D., Baugh, K.E., Kihn, E.A., Kroehl, H.W., Davis, E.R., Davis, C.W., 1997. Relation between satellite observed visible-near infrared emissions, population, economic activity and electric power consumption. Int. J. Remote Sens. 18 (6), 1373–1379. https://doi.org/10.1080/014311697218485.
Gaston, K.J., Bennie, J., Davies, T.W., Hopkins, J., 2013. The ecological impacts of nighttime light pollution: a mechanistic appraisal. Biol. Rev. 88 (4), 912–927. https://doi.org/10.1111/brv.12036.
Geldmann, J., Joppa, L.N., Burgess, N.D., 2014. Mapping Change in Human Pressure Globally on Land and within Protected Areas. Conserv. Biol. 28 (6), 1604–1616. https://doi.org/10.1111/cobi.12332.
Ghosh, T., Anderson, S., Powell, R.L., Sutton, P.C., Elvidge, C.D., 2009. Estimation of Mexico's informal economy and remittances using nighttime imagery. Remote Sensing 1, 418–444. https://doi.org/10.3390/rs1030418.
Ghosh, T., Elvidge, C.D., Sutton, P.C., Baugh, K.E., Ziskin, D., Tuttle, B.T., 2010. Creating a global grid of distributed fossil fuel CO_2 emissions from nighttime satellite imagery. Energies 3 (12), 1895–1913. https://doi.org/10.3390/en3121895.
Green, D.S., Zipkin, E.F., Incorvaia, D.C., Holekamp, K.E., 2019. Long-term ecological changes influence herbivore diversity and abundance inside a protected area in the Mara-Serengeti ecosystem. Global Ecol. Conserv. 20, e00697. https://doi.org/10.1016/j.gecco.2019.e00697.
He, C., Shi, P., Li, J., Chen, J., Pan, Y., Li, J., Zhuo, L., Ichinose, T., 2006. Restoring urbanization process in China in the 1990s by using non-radiance-calibrated DMSP/OLS nighttime light imagery and statistical data. Chin. Sci. Bull. 51 (13), 1614–1620. https://doi.org/10.1007/s11434-006-2006-3.
Henderson, M., Yeh, E.T., Gong, P., Elvidge, C., Baugh, K., 2003. Validation of urban boundaries derived from global night-time satellite imagery. Int. J. Remote Sens. 24 (3), 595–609. https://doi.org/10.1080/01431160304982.
Hu, Y., Chen, J., Cao, X., Chen, X., Cui, X., Gan, L., 2021. Correcting the Saturation Effect in DMSP/OLS Stable Nighttime Light Products Based on Radiance-Calibrated Data. IEEE Transactions on Geoscience and Remote Sensing 1–11. https://doi.org/10.1109/TGRS.2021.3060170.
Jones, K.R., Venter, O., Fuller, R.A., Allan, J.R., Maxwell, S.L., Negret, P.J., Watson, J.E. M., 2018. One-third of global protected land is under intense human pressure. Science 360 (6390), 788–791. https://doi.org/10.1126/science.aap9565.
Joppa, L. N., Loarie, S. R., Pimm, S. L., 2008. On the protection of "protected areas". Proceedings of the National Academy of Sciences 105 (18), 6673-6678. 10.1073/pnas.0802471105.
Levin, N., 2017. The impact of seasonal changes on observed nighttime brightness from 2014 to 2015 monthly VIIRS DNB composites. Remote Sens. Environ. 193, 150–164. https://doi.org/10.1016/j.rse.2017.03.003.
Li, X., Li, D., Xu, H., Wu, C., 2017. Intercalibration between DMSP/OLS and VIIRS night-time light images to evaluate city light dynamics of Syria's major human settlement during Syrian Civil War. Int. J. Remote Sens. 38 (21), 5934–5951. https://doi.org/10.1080/01431161.2017.1331476.
Li, X., Zhou, Y., Zhao, M., Zhao, X., 2020. A harmonized global nighttime light dataset 1992–2018. Sci. Data 7, 168. https://doi.org/10.1038/s41597-020-0510-y.
Liu, Z., Wang, Y., Yao, Z., Kang, H., 2011. Trend and Periodicity of Precipitation, Air Temperature and Runoff in the Taihu Lake Basin. Journal of Natural Resources 26 (09), 1575-1584. 10.11849/zrzyxb.2011.09.013.
Longcore, T., Rich, C., 2004. Ecological light pollution. Front. Ecol. Environ. 2 (4), 191–198. https://doi.org/10.1890/1540-9295(2004)002[0191:ELP]2.0.CO;2.
Lu, D., Tian, H., Zhou, G., Ge, H., 2008. Regional mapping of human settlements in southeastern China with multisensor remotely sensed data. Remote Sens. Environ. 112 (9), 3668–3679. https://doi.org/10.1016/j.rse.2008.05.009.
Ma, J., Guo, J., Ahmad, S., Li, Z., Hong, J., 2020. Constructing a new inter-calibration method for DMSP-OLS and NPP-VIIRS nighttime light. Remote Sensing 12 (6), 937. https://doi.org/10.3390/rs12060937.
Mammides, C., 2020. A global assessment of the human pressure on the world's lakes. Global Environ. Change 63, 102084. https://doi.org/10.1016/j.gloenvcha.2020.102084.
Navara, K.J., Nelson, R.J., 2007. The dark side of light at night: physiological, epidemiological, and ecological consequences. J. Pineal Res. 43 (3), 215–224. https://doi.org/10.1111/jpi.2007.43.issue-310.1111/j.1600-079X.2007.00473.x.
Perkin, E.K., Hölker, F., Richardson, J.S., Sadler, J.P., Wolter, C., Tockner, K., 2011. The influence of artificial light on stream and riparian ecosystems: questions, challenges, and perspectives. Ecosphere 2 (11), 1–16. https://doi.org/10.1890/ES11-00241.1.
Rich,C., Longcore, T., 2006. Introduction. In Ecological Consequences of Artificial Night Lighting (eds C. Rich and T. Longcore), Island Press, Washington (pp. 1-13).
Riggio, J., Jacobson, A.P., Hijmans, R.J., Caro, T., 2019. How effective are the protected areas of East Africa? Global Ecol. Conserv. 17, e00573. https://doi.org/10.1016/j.gecco.2019.e00573.
Román, M.O., Wang, Z., Sun, Q., Kalb, V., Miller, S.D., Molthan, A., Schultz, L., Bell, J., Stokes, E.C., Pandey, B., Seto, K.C., Hall, D., Oda, T., Wolfe, R.E., Lin, G., Golpayegani, N., Devadiga, S., Davidson, C., Sarkar, S., Praderas, C., Schmaltz, J., Boller, R., Stevens, J., Ramos González, O.M., Padilla, E., Alonso, J., Detrés, Y., Armstrong, R., Miranda, I., Conte, Y., Marrero, N., MacManus, K., Esch, T., Masuoka, E.J., 2018. NASA's Black Marble nighttime lights product suite. Remote Sens. Environ. 210, 113–143. https://doi.org/10.1016/j.rse.2018.03.017.
Shi, K., Huang, C., Chen, Y., Li, L., 2018. Remotely sensed nighttime lights reveal increasing human activities in protected areas of China mainland. Remote Sensing Letters 9 (5), 467–476. https://doi.org/10.1080/2150704X.2018.1439199.
Shi, K., Yu, B., Huang, Y., Hu, Y., Yin, B., Chen, Z., Chen, L., Wu, J., 2014. Evaluating the ability of NPP-VIIRS nighttime light data to estimate the gross domestic product and the electric power consumption of China at multiple scales: A comparison with DMSP-OLS data. Remote Sensing 6 (2), 1705–1724. https://doi.org/10.3390/rs6021705.
Sutton, P., 1997. Modeling population density with night-time satellite imagery and GIS. Comput. Environ. Urban Syst. 21 (3–4), 227–244. https://doi.org/10.1016/S0198-9715(97)01005-3.
Sutton, P.C., Costanza, R., 2002. Global estimates of market and non-market values derived from nighttime satellite imagery, land cover, and ecosystem service valuation. Ecol. Econ. 41 (3), 509–527. https://doi.org/10.1016/S0921-8009(02)00097-6.
Tucker, C.J., Newcomb, W.W., Los, S.O., Prince, S.D., 1991. Mean and inter-year variation of growing-season normalized difference vegetation index for the Sahel 1981–1989. Int. J. Remote Sens. 12 (6), 1133–1135. https://doi.org/10.1080/01431169108929717.
Venter, O., Sanderson, E.W., Magrach, A., Allan, J.R., Beher, J., Jones, K.R., Possingham, H.P., Laurance, W.F., Wood, P., Fekete, B.M., Levy, M.A., Watson, J.E. M., 2016. Sixteen years of change in the global terrestrial human footprint and implications for biodiversity conservation. Nat. Commun. 7, 12558. https://doi.org/10.1038/ncomms12558.
Waluda, C.M., Yamashiro, C., Elvidge, C.D., Hobson, V.R., Rodhouse, P.G., 2004. Quantifying light-fishing for Dosidicus gigas in the eastern Pacific using satellite remote sensing. Remote Sens. Environ. 91 (2), 129–133. https://doi.org/10.1016/j.rse.2004.02.006.
Watson, J.E.M., Venter, O., Lee, J., Jones, K.R., Robinson, J.G., Possingham, H.P., Allan, J.R., 2018. Protect the last of the wild. Nature 563 (7729), 27–30. https://doi.org/10.1038/d41586-018-07183-6.
Wei, J., He, G., Long, T., Wang, C., Ni, Y., Ma, R., 2017. Assessing light pollution in China based on nighttime light imagery. Remote Sensing 9, 135. https://doi.org/10.3390/rs9020135.
Wu, K., Wang, X., 2019. Aligning pixel values of DMSP and VIIRS nighttime light images to evaluate urban dynamics. Remote Sensing 11 (12), 1463. https://doi.org/10.3390/rs11121463.
WWF.,, 2020. Living Planet Report 2020: Bending the curve of biodiversity loss. In: Almond, R.E.A., Grooten, M., Petersen, T. (Eds.), WWF. Switzerland, Gland, pp. 6–7.
Xiang, W., Tan, M., 2017. Changes in light pollution and the causing factors in China's protected areas, 1992–2012. Remote Sensing 9 (10), 1026. https://doi.org/10.3390/rs9101026.
Xu, Pengfei, Wang, Quan, Jin, Jia, Jin, Pingbin, 2019. An increase in nighttime light detected for protected areas in mainland China based on VIIRS DNB data. Ecol. Ind. 107, 105615. https://doi.org/10.1016/j.ecolind.2019.105615.
Yang, H., Xu, H., 2019. Assessing fractional vegetation cover changes and ecological quality of the Wuyi mountain national nature reserve based on remote sensing spatial information. Chin. J. Appl. Ecol. 31 (2), 533–542. https://doi.org/10.13287/j.1001-9332.202002.014.
Yu, B., Shu, S., Liu, H., Song, W., Wu, J., Wang, L., Chen, Z., 2014. Object-based spatial cluster analysis of urban landscape pattern using nighttime light satellite images: A case study of China. International Journal of Geographical Information Science 28 (11), 2328–2355. https://doi.org/10.1080/13658816.2014.922186.
Zhang, M., Liu, Q., Wang, J., Cai, Y., Bai, Z., Ye, J., 2020. Monitoring Human Activities in Jiaozi Mountain Nature Reserve Based on Remote Sensing During 1992–2018. Journal of Ecology and Rural Environment 36 (09), 1097–1110. https://doi.org/10.19741/j.issn.1673-4831.2019.1002.
Zhao, Min, Zhou, Yuyu, Li, Xuecao, Zhou, Chenghu, Cheng, Weiming, Li, Manchun, Huang, Kun, 2020. Building a Series of Consistent Night-Time Light Data (1992–2018) in Southeast Asia by Integrating DMSP-OLS and NPP-VIIRS. IEEE Trans. Geosci. Remote Sens. 58 (3), 1843–1856. https://doi.org/10.1109/TGRS.3610.1109/TGRS.2019.2949797.
Zheng, Q., Weng, Q., Wang, K., 2019a. Developing a new cross-sensor calibration model for DMSP-OLS and Suomi-NPP VIIRS night-light imageries. ISPRS J. Photogramm. Remote Sens. 153, 36–47. https://doi.org/10.1016/j.isprsjprs.2019.04.019.
Zheng, Qiming, Weng, Qihao, Wang, Ke, 2020a. Correcting the Pixel Blooming Effect (PiBE) of DMSP-OLS nighttime light imagery. Remote Sens. Environ. 240, 111707. https://doi.org/10.1016/j.rse.2020.111707.
Zheng, Z., Wu, Z., Chen, Y., Yang, Z., Marinello, F., 2020b. Exploration of eco-environment and urbanization changes in coastal zones: A case study in China over the past 20 years. Ecol. Ind. 119, 106847 https://doi.org/10.1016/j.ecolind.2020.106847.
Zheng, Z., Yang, Z., Chen, Y., Wu, Z., Marinello, F., 2019b. The Interannual Calibration and Global Nighttime Light Fluctuation Assessment Based on Pixel-Level Linear Regression Analysis. Remote Sensing 11 (18), 2185. https://doi.org/10.3390/rs11182185.
Zhu, P., Huang, L., Xiao, T., Wang, J., 2018. Dynamic changes of habitats in China's typical nature reserve on spatial and temporal scales. Acta Geographica Sinica 73 (1), 92–103. https://doi.org/10.11821/dlxb201801008.
Zhuo, L., Ichinose, T., Zheng, J., Chen, J., Shi, P.J., Li, X., 2009. Modelling the population density of China at the pixel level based on DMSP/OLS non-radiance-calibrated night-time light images. Int. J. Remote Sens. 30 (4), 1003–1018. https://doi.org/10.1080/01431160802430693.